High Quantum Yield Nitrogen-Carbon Dots (N-CDs) from Plastic Waste

Lestari, Ratih
Department of Chemistry, Faculty of Mathematics and Natural Sciences, Universitas Gadjah Mada

Tutik Dwi Wahyuningsih
Department of Chemistry, Faculty of Mathematics and Natural Sciences, Universitas Gadjah Mada

Kartini, Indriana
Department of Chemistry, Faculty of Mathematics and Natural Sciences, Universitas Gadjah Mada

https://doi.org/10.5109/7151677

出版情報：Evergreen. 10 (3), pp.1313-1322, 2023-09. 九州大学グリーンテクノロジー研究教育センター
バージョン：

High Quantum Yield Nitrogen-Carbon Dots (N-CDs) from Plastic Waste

Ratih Lestari, Tutik Dwi Wahyuningsih, Indriana Kartini*
Department of Chemistry, Faculty of Mathematics and Natural Sciences, Universitas Gadjah Mada, Yogyakarta 55281, Indonesia

*Author to whom correspondence should be addressed:
E-mail: indriana@ugm.ac.id

(Received June 11, 2023; Revised September 16, 2023; accepted September 19, 2023).

Abstract: A high quantum yield of up to 20% N-CDs from plastic bag waste has been synthesized via the pyrolysis-hydrothermal method. Using plastic bag waste as a carbon source offers several advantages, including their abundant availability, low cost, and potential to reduce plastic waste in the environment. The effect of hydrothermal time and H_2O_2 concentration as an oxidant was evaluated. The N-CDs acquired exhibit a consistent blue fluorescence, possess an average dimension of 5.94 nm, and consist of graphitic structures that may contain flaws induced by surface functional groups such as amine, imine, alcohol, carboxyl, and carbonyl. Excellent stability of the resulting N-CD toward storage time, NaCl, and phosphate buffered salt (PBS) solution pave the way to possible applications for metal ions sensing in wastewater and human cells.

Keywords: fluorescence; hydrothermal; Nitrogen-carbon dots; pyrolysis; plastic bag waste

1. Introduction

The growing need for plastic has been accompanied by an upsurge in its manufacturing. Plastic possesses durable qualities and strong stability, which pose challenges to its decomposition in the environment. It is estimated that around 80% of the total plastic waste ever produced has gathered in natural ecosystems or ended up in landfills[1], then potentially becomes a problem for ecosystems and public health[2]. Therefore, plastic management is important to minimize the plastic waste quantity in the environment. Plastic bags contribute significantly to environmental pollution, as they can endure for centuries without decomposing and pose a threat to animals and marine ecosystems[3]. Due to the high carbon content up to 84.74%[4], plastic bag wastes have the potential as the source of carbon dots (CDs). Converting plastic bags into CDs can help mitigate these environmental impacts and represents an innovative solution to the problem of plastic waste. This process inspires new ideas and approaches to sustainability and encourages further research and development in this field.

Researchers are captivated by the remarkable characteristics of CDs, including their fluorescence capability, excellent stability, minimal toxicity, strong compatibility with living organisms, and their ability to act as both electron donors and acceptors[5]. These unique properties make CDs highly promising for a diverse array of applications, such as bio-imaging[6], drug delivery[7], contaminant detection[8], LED[9], solar cells[10], photocatalysis[11], and corrosion inhibitors[12].

The synthesis of CDs by subjecting waste plastic bags to hydrothermal conditions at 180 °C for 12 h has been investigated by Hu et al.[4]. CDs obtained have a quantum yield of 4.08% and exhibited blue fluorescence under UV light. Another study by Hu et al.[13] involved synthesizing CDs from waste PET through pyrolysis (350 °C, 2 h) and hydrothermal (180 °C, 12 h) using H_2O_2 as an oxidant. The CDs obtained in this case displayed a vigorous blue fluorescence and 5.2% quantum yield. Kumari et al.[14] employed a modified technique involving sonication and hydrothermal methods to synthesize CDs from polyolefin waste. The resulting product exhibited a robust green fluorescence, achieving a quantum yield of up to 4.84%. However, despite these findings, the CDs derived from plastic waste suffer from a relatively low quantum yield, typically below 5.2%.

Several studies have focused on enhancing the CDs quantum yield[15,16]. Fluorescence properties of CDs can originate from various factors, including surface states such as the level of surface oxidation and the presence of functional groups[5], quantum confinement effect[17], or the synergistic effect of both of them[18]. Consequently, modifying functional groups on the CDs surface can enhance the quantum yield.

Manioudakis et al.[15] conducted a modification on citric acid-based carbon dots (CDs) by introducing nitrogen from diethylenetriamine. This led to the creation of N-CDs that displayed blue-green fluorescence and had a

remarkable quantum yield of 56.70%, which is 56 times higher than that of the pristine CDs. Similarly, Fu et al.[19] passivated CDs from citric acid with nitrogen from ethylenediamine, resulting in N-CDs with high quantum yield (67.40%) and robust blue fluorescence. N-CDs have also been synthesized from polyethylene terephthalate (PET) plastic using combined reflux and hydrothermal methods[16]. However, it was discovered that N-CDs have a quantum yield of 9.1%.

This study presents the N-CDs production with noteworthy quantum yield from high-density polyethylene (HDPE) plastic bag waste. HDPE plastic was chosen because it consists of a C-C backbone polymer, which is more widely produced at approximately 77% compared to heteroatomic polymers[20]. Plastics composed of this C-C backbone polymer are not easily degraded, resulting in a large availability. Additionally, HDPE plastic contains a higher carbon content, reaching 84.74%, compared to other C-C backbone plastics like LDPE and PVC[4,21]. This enhances the potential of HDPE plastic for use as a raw material in CD production. We utilized a combination method involving pyrolysis and hydrothermal processes. Urea served as the source of nitrogen due to its availability and reactivity compared to other nitrogen sources, while H_2O_2 was used as an oxidizing agent. We opted for the pyrolysis-hydrothermal approach instead of the reflux-hydrothermal method, as pyrolysis enables the breakdown of plastic polymer chains into simpler chains without the need for solvents. Consequently, this method yields a purer product compared to the reflux-hydrothermal method as reflected by the high value of the quantum yield.

2. Materials and Methods

2.1 Materials

Hydrogen peroxide (30 wt.% H_2O_2), urea, quinine sulfate, phosphate buffered salt (1X PBS, pH 7.4), and sodium chloride were purchased from Merck (Germany). Carbon sources for the experiment were HDPE plastic bags manufactured by Santoso Company. All substances were of high purity without necessitating additional purification.

2.2 Synthesis of N-CDs

Table 1. Optimization parameters for N-CDs synthesis from plastic bags with a urea mass of 0.125 g except N-CDs 0.

H_2O_2 Conc. (wt.%)	Hydrothermal Time (h)	Symbol	QY (%)
0	6	N-CDs 06	1.2
3	6	N-CDs 36	17.0
5	6	N-CDs 56	20.0
5	4	N-CDs 54	10.0
5	2	N-CDs 52	2.5
5	6	N-CDs 0	3.6

N-CDs were produced by pyrolyzing 1 g of HDPE plastic bags at 300 °C for 4 h. Then, about 0.250 g of pyrolyzed product was combined with 15 mL of H_2O_2 and urea, according to Table 1. The resulting mixture was then transferred to a 25 mL autoclave. After the hydrothermal process was conducted at 180 °C at various times (Table 1), the solution was centrifugated at 4,000 rpm for around 30 min to eliminate any residues. Ultimately, the yield of N-CDs obtained ranged from 6.9% to 30.2%. Modification CDs with nitrogen, increasing the H_2O_2 concentration from 0 to 5 wt%, and extending the hydrothermal time from 2 to 6 h can enhance the yield of the resulting CDs. Furthermore, N-CDs obtained have blue fluorescence under UV light and a pale-yellow transparent appearance under daylight, as shown in the inset of Fig. 2.

2.3 Characterization of N-CDs

Before optical properties analysis, 0.1 mL of N-CDs was dissolved in 3 mL of deionized water and then characterized using a UV-Vis Shimadzu and RF-6000 fluorescence spectrometer. The wavelength range was 200-800 nm for UV-Vis spectra, while for fluorescence spectra, emission wavelengths ranged from 300-600 nm and 300-420 nm for excitation wavelengths.

The quantum yield (QY) measurement was conducted on the N-CDs 56 using the following equation:

$$\varphi_{N\text{-}CDs} = \varphi_R \cdot I_{N\text{-}CDs}/I_R \cdot A_R/A_{N\text{-}CDs} \cdot \eta^2_{N\text{-}CDs}/\eta^2_R \qquad (1)$$

In the equation, "φ" represents quantum yield, "I" represents fluorescence intensity, "A" represents absorbance, and "η" represents the refractive index of the solvent used, which is water (1.33). The subscript "N-CDs and R" mention the N-CDs and the reference, respectively. Quinine sulfate is employed as the reference compound, possessing a quantum yield of 54%[15].

The optical stability was determined based on fluorescence intensity changes of N-CDs 56 at three different conditions, namely after being stored for up to 54 days, after adding NaCl at various concentrations (0.0; 0.5; 1; and 1.5 M), and PBS solution at various concentrations (0; 25; 50; and 100%), separately. The procedure involved the addition of 0.1 mL of N-CDs 56 to 3 mL of deionized water to determine the storage stability, NaCl and PBS solution to determine the ion strength stability. Then, the solution was characterized using fluorescence spectroscopy at 320 nm as the excitation wavelength.

XRD analysis was conducted on dried N-CD samples using a Bruker D2 Phaser XRD. The FTIR spectra were acquired by the Shimadzu FTIR spectrometer, covering the wavenumber from 4000 to 400 cm^{-1}. Raman spectra were acquired using the iHR320 instrument, employing an excitation wavelength laser of 532 nm. The zeta potential was measured utilizing a Nano Series Malvern Zetasizer instrument, maintaining at 25 ˚C, a count rate of 90.1 kcps, and performing 12 zeta runs. TEM, EDS, and SAED

characterization were executed using a TEM FEI Technai G2 20 S-Twin with a voltage of 200 kV. Image analysis and particle size calculations were conducted using J-Image software.

3. Results and Discussion

3.1 Synthesis of N-CDs

The optimal method to convert plastic bags into N-CDs was determined by examining the optical properties of N-CDs. Fig. 1 displayed the UV-Visible spectra of N-CDs and a maximum absorption band was observed at around 289 to 300 nm assigned to electron transition of π-π* from the carbonic core, which suggested the conjugated system of C=C in the N-CDs structure[6,14]. The broad absorption up to 500 nm referred to the presence of electron excitation from n-π* attributed to the heteroatomic surface functionalities of N-CDs[9,22]. Furthermore, based on UV-Visible spectra, the rise of H_2O_2 concentration as an oxidant from 0 (N-CDs 06) to 3 (N-CDs 36) and up to 5 wt.% (N-CDs 56) can increase the absorbance of CDs obtained and cause the absorption band to broaden towards longer wavelengths. This is due to the rise of H_2O_2 concentration which can increase the functional group's quantity of CDs surface[11]. H_2O_2 contains oxygen and will add oxygen groups on the CDs surface. These functional groups can trap excited state energies, which may help in achieving strong fluorescence. The concentration of H_2O_2 that produced the highest absorbance CDs was 5 wt.% (N-CDs 56).

A variation in the hydrothermal time was performed to determine the optimal synthesis time for producing N-CDs with the best optical properties. Increasing the hydrothermal time from 2 to 6 h (N-CDs 52, N-CDs 54, and N-CDs 56) can enhance the absorbance and cause the absorption band to broaden towards longer wavelengths. This was because increasing the hydrothermal time can optimize the breakdown of plastic and urea chains, forming oxidized species that will be passivated on the CDs surface[8]. The use of 6 h hydrothermal time (N-CDs 56) was the best time for producing N-CDs with the highest absorbance. Compared to CDs without nitrogen doping (N-CDs 0), N-CDs 56 had higher absorbance. This occurrence is possible due to urea's ability to introduce oxygen and nitrogen groups onto the CDs surface.

The emission spectra in Fig. 2 showed that the highest intensity peaked at 415 nm upon excitation wavelength at 320 nm. As the concentration of H_2O_2 increased from 0 to 5 wt.%, (N-CDs 06, N-CDs 36, and N-CDs 56) exhibited an upward trend. This trend aligned with the observed increase in absorbance measured by UV-Visible spectrophotometer. Notably, the highest fluorescence intensity of N-CDs was obtained using 5 wt.% H_2O_2 (N-CDs 56). Moreover, by extending the hydrothermal time from 2 to 6 h, the fluorescence intensity of the N-CDs was further enhanced. This improvement can be attributed to the optimized presence of heteroatom functional groups on the CDs surface. Specifically, a hydrothermal time of 6 h (N-CDs 56) was found to produce CDs with the maximum fluorescence intensity. Passivation of nitrogen onto CDs can increase fluorescence intensity compared to the pristine CDs (N-CDs 0).

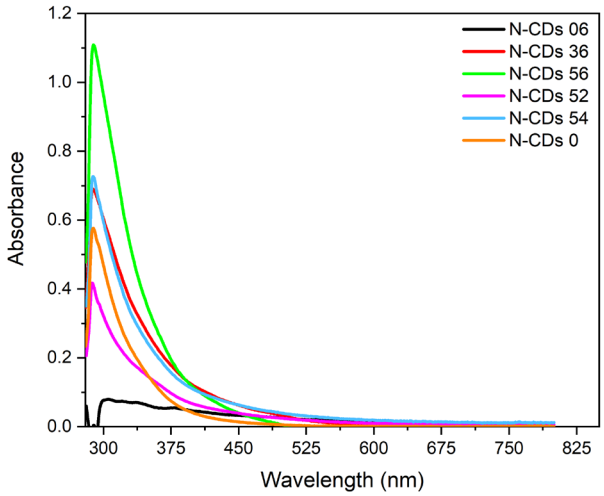

Fig. 1: UV-Vis spectra of N-CDs at different H_2O_2 concentrations and hydrothermal time.

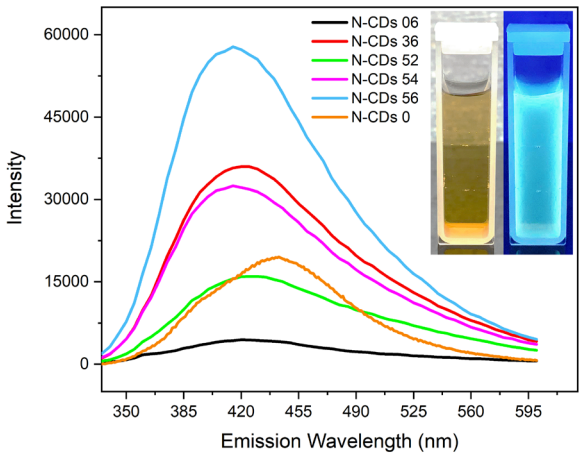

Fig. 2: Emission spectra of N-CDs at different hydrogen peroxide concentrations and hydrothermal time (Inset shows the photograph of N-CDs under UV irradiation (right) and daylight (left)).

Table 2. N-CDs quantum yield from plastic as the precursor.

Sources	Nitrogen precursor	Additional chemicals	Method	QY (%)	Ref.
Polyethylene terephthalate (PET)	Diethylenetriamine (DETA)	H_2O_2 and zinc acetate	Reflux-Hydrothermal	9.10	16)
Waste-expanded polystyrene (EPS)	Ethylene-diamine (EDA)	$CHCl_3$	Solvothermal	20.00	23)
Polyurethane (PU)	-	H_2SO_4	Pyrolysis	33.00	24)
Polyethylene terephthalate (PET)	Urea	Ethylene glycol, zinc acetate, pyromellitic anhydride, and THF	Thermal-Solvothermal	48.16	25)
Plastic bag (HDPE)	Urea	H_2O_2	Pyrolysis-Hydrothermal	20.00	This work

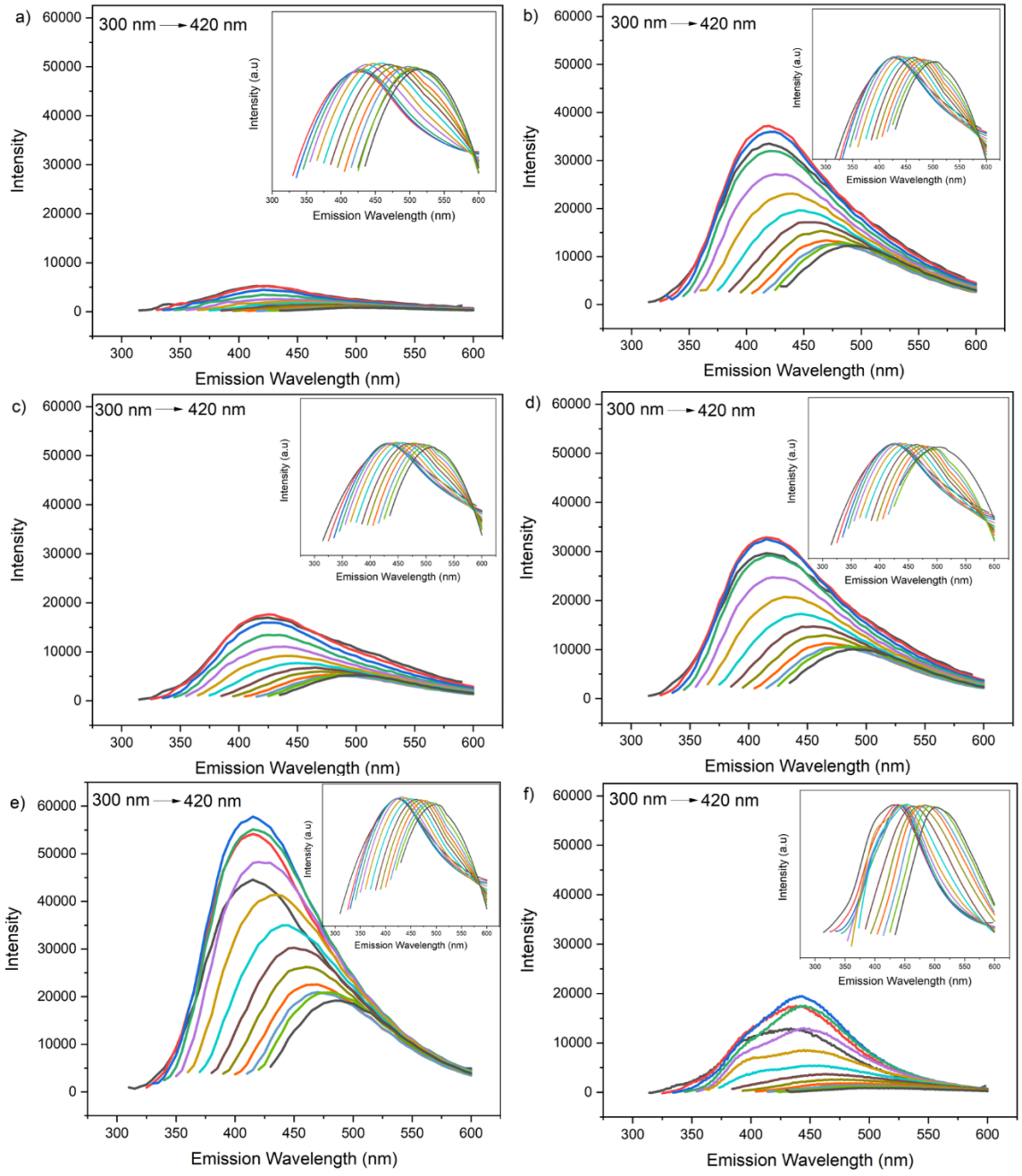

Fig. 3: Emission spectra at varying excitation wavelengths from 300 to 420 nm (10 nm increment) for a) N-CDs 06; b) N-CDs 36; c) N-CDs 52; d) N-CDs 54; e) N-CDs 56; f) N-CDs 0. (Inset shows the normalization of emission spectra).

The determination of quantum yield was then performed on all N-CDs obtained using the quinine sulfate as the reference. N-CDs 06, N-CDs 36, N-CDs 54, N-CDs 52, and N-CDs 0 have a quantum yield of 1.2, 17, 10, 2.5, and 3.6%, respectively (Table 1). N-CDs 56 has the highest quantum yield of 20%. The increase in quantum yield is in line with the rise of fluorescence intensity. Table 2 shows the quantum yield comparison from plastic-based N-CDs. The use of the pyrolysis-hydrothermal method can generate a higher quantum yield than the reflux-hydrothermal method, as expected. However, the quantum yield value is also influenced by the presence of nitrogen precursor types and other additional chemicals, as shown in the research findings of Ma et al.[25].

The fluorescence spectra in Fig. 3 revealed that the emission intensity grows at excitation wavelengths, changing from 300 to 320 nm. The intensity of fluorescence decreases as the excitation wavelength shifts from 330 to 420 nm, indicating that 320 nm is the maximum excitation wavelength. In addition, Fig. 3 also shows a redshift of the emission peak with an increase in excitation wavelength from 300 to 420 nm with a 10 nm increment. This suggests that N-CDs have a unique character of excitation-dependent emission wavelength, which is commonly exhibited by carbon nanomaterials that can fluorescence. The emission wavelength of N-CDs shifted from 415 to 510 nm, indicating the excitation-dependent emission behavior noticed. It is primarily influenced by the various surface states rather than the quantum confinement effect[23]. Surface functional groups play a crucial role in the fluorescence properties. The introduction of heteroatom groups, such as nitrogen, to the surface of CDs can stabilize surface energy traps and enhance the fluorescence properties of N-CDs. Nitrogen-rich atoms in N-CDs are particularly important in generating the excitation-dependent fluorescence observed[26].

Fig. 4 shows the FTIR spectra of N-CDs with various synthesis parameters. N-CDs 0 (Fig. 4a) has absorptions at ~3400 cm^{-1} belonging to -OH stretching, ~2850 and 2930 cm^{-1} assigning to C-H sp^3, ~1700 due to of C=O stretching, ~1603 cm^{-1} are related to C=C stretching of aromatic groups, and ~1162 cm^{-1} due to O-C-O stretching[13]. Passivation CDs with urea and H_2O_2 3 wt.% as oxidants (Fig. 4b) caused a broadening peak at 3200-3500 cm^{-1}, overlapping peaks at 1500-1750 cm^{-1}, and an additional absorption emerged at ~1404 cm^{-1}. The broadening of the absorption band at 3200-3500 cm^{-1} was attributed to the overlapping vibrations of hydroxyl (O-H) and amine (N-H) groups. Furthermore, the broadening of the absorption band at ~1500-1750 cm^{-1} corresponds to the overlapping C=C, C=O, and C=N groups vibration, while the absorption at 1404 cm^{-1} indicates the presence of a C-N absorption [27,28]. It indicated that passivation CDs with nitrogen could add the heteroatom functional groups on the CDs surface, such as C=N, N-H, and C-N.

The synthesis time variation between 2 and 4 h did not show remarkable differences in the FTIR spectra (Fig. 4c and 4d). However, upon increasing the hydrothermal time to 6 h and the H_2O_2 concentration to 5 wt.%, the absorption band around 3200-3500 and 1500-1750 cm^{-1} were observed to become broader in Fig. 4e, suggesting the abundance of N-H and O-H groups present on N-CDs surface. Furthermore, at ~1500-1750 cm^{-1} the absorption band also broadened, referred to the additional C=N and C=O groups. There was also a peak at ~1180 cm^{-1} due to O-C-O stretching. It is assumed that the use of hydrothermal time is 6 h and H_2O_2 concentration 5 wt.% (N-CDs 56) can increase the functional groups of oxygen and nitrogen. These groups contribute to obtaining N-CDs with optimal fluorescence intensity. Additionally, the presence of these groups can cause N-CDs to have hydrophilic properties and high solubility in water, making them potentially applicable in various fields such as sensors and bio-imaging.

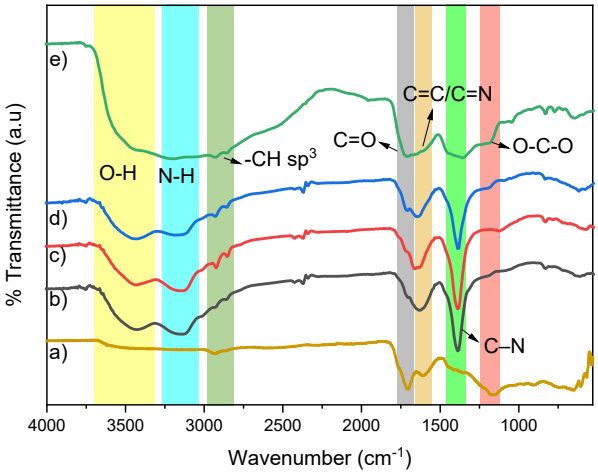

Fig. 4: FTIR spectra of a) N-CDs 0; b) N-CDs 36; c) N-CDs 52; d) N-CDs 54; e) N-CDs 56.

The characterization of the optical stability is conducted because it greatly influences the effectiveness of N-CDs for long-term application (eg. solar cells). In this study, the N-CDs stability was tested regarding storage time, and the presence of NaCl and PBS. Generally, the fluorescence intensity can decrease as the storage time increases[14]. Additionally, the presence of NaCl can also reduce the fluorescence intensity as it easily binds to the functional groups on N-CDs surface, rendering them ineffective when applied in salt-containing media, such as sensor and bio-imaging. The optical stability of N-CDs 56 was tested after storing for up to 54 days and adding NaCl solution. Based on Fig. 5a, N-CDs 56 obtained showed good stability after being stored for up to 54 days. This is indicated by the fluorescence intensity that did not significantly change with storage for up to 54 days. Additionally, there was no observed aggregation during the 54-day storage period. Hence, the N-CD particles have good stability. The addition of NaCl solution to N-CDs 56 was performed to identify the fluorescence intensity

change caused by the ionic strength presence. There was no significant change in fluorescence intensity with NaCl addition from 0 to 1.5 M (Fig. 5b). This result expressed that N-CDs aggregation can be effectively controlled by the strength of NaCl ions and can be separated even in the existence of interfering salts. The N-CDs 56 solution remained homogenous without visible precipitation upon the addition of NaCl, as there was no ionization of surface functional groups of N-CDs 56 in the existence of NaCl. This suggests that N-CDs 56 is suitable for use in harsh and sophisticated conditions. The fluorescence stability of N-CDs 56 was also investigated in phosphate-buffered saline (PBS) at various concentrations of 0; 25; 50; and 100% (Fig. 5c) to indicate the tolerability of N-CDs in human cells. Increasing the PBS concentration up to 50% did not lead to significant changes in fluorescence intensity, indicating good fluorescence stability of N-CDs. However, raising the PBS concentration to 100% resulted in a slight decrease in fluorescence intensity, of about 10%. The decrease could be due to interactions between the surface functional groups of N-CDs (carboxyl, carbonyl, hydroxyl, and amine) with the cations in PBS such as K^+ and Na^+. This finding suggests that the resulting N-CDs have the potential to be applied in studies involving human cells.

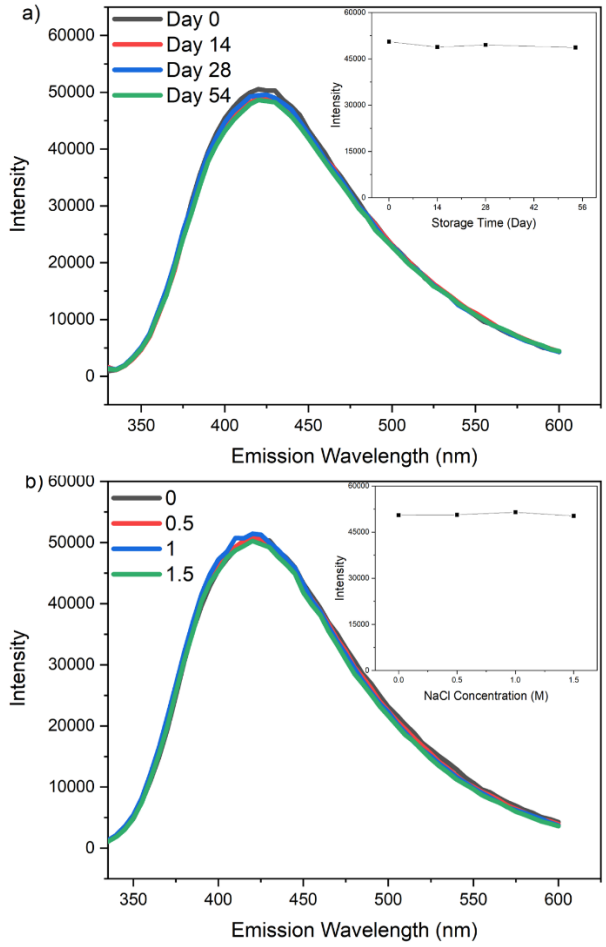

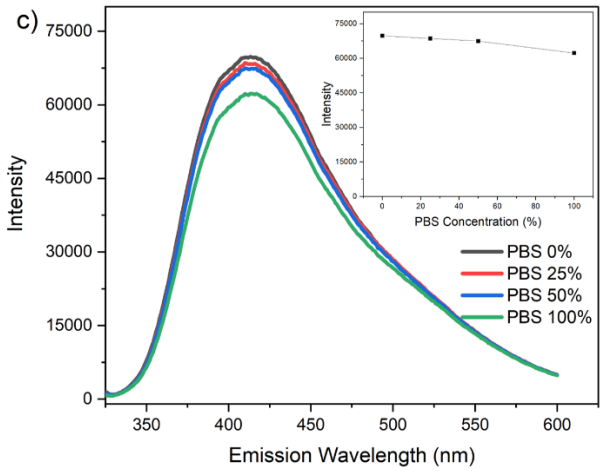

Fig. 5: Emission spectra of N-CDs 56 a) after storage for 54 days, b) after the addition of NaCl with varying concentrations, and c) after the addition of PBS with different concentrations. (Inset shows the graph of N-CDs stability over storage time (a), NaCl concentration (b), and PBS concentration c) at excitation and emission wavelengths of 320 and 420 nm, respectively).

3.2 Structure of N-CDs

According to the FTIR spectra in Fig. 4d, N-CDs 56 have functional groups such as alcohol, carbonyl, carboxyl, amine, and imine. Based on the XRD pattern in Fig. 6, N-CDs 56 have a low degree of crystallinity, indicating amorphous structures. The peak observed at 2θ = 27.9° with an interplanar distance of 0.32 nm depicts the graphite (002) structure (JCPDS 00-012-0212)[29]. The (002) orientation corresponds to the vertical axis, or c-axis, of the graphite unit cell, which is oriented perpendicular to the hexagonal planes. The interplanar distance is slightly shorter than graphite (002) (0.34 nm), probably due to closely packed carbon atoms with surface functionalities. In addition, a peak at 17.2°, corresponds to an interplanar distance of 0.52 nm. The increased interplanar distance compared to graphite (002) may be due to the presence of defects in the graphite lattice caused by bonding with oxygen or nitrogen functional groups[13]. This is consistent with FTIR that N-CDs contained alcohol, carboxyl, carbonyl, amine, and imine. An additional peak at 2θ = 42.1° with an interplanar distance of 0.19 nm belongs to graphite with the lattice (101)[30].

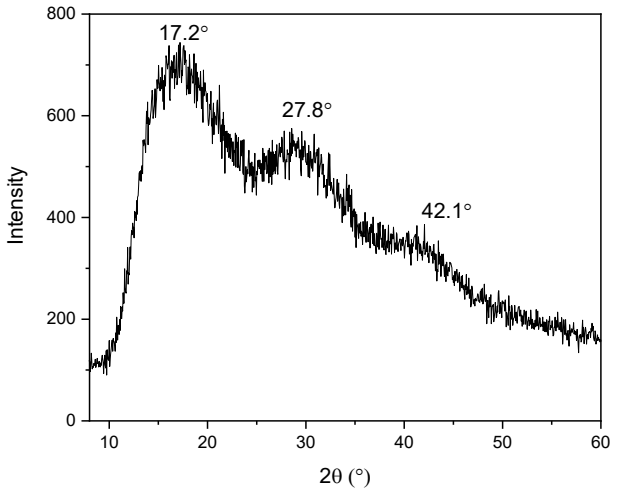

Fig. 6: XRD pattern of N-CDs 56

In Fig. 7, the Raman spectrum of N-CDs 56 shows the absorption band at 1232 cm^{-1}, indicating the D band, and a broad peak at 1591 cm^{-1} belonging to the G band existence. The appearance of both D and G bands indicates a carbonaceous structure of N-CDs 56[31]. The D band is accompanied by edge defects and disorder in the carbon lattice. The G band represents sp^2 carbon atoms the vibrational within the graphene planes and indicates the crystalline structure of the carbon materials. The D band intensity is much greater than the G band, which means that N-CDs 56 structures have low crystallinity and are accordant with the XRD pattern. The low crystallinity was probably due to surface defects caused by alcohol, carboxyl, carbonyl, amine, and imine groups which also confirmed with FTIR. The Raman spectrum confirms that N-CDs 56 consist of a graphitic structure with defects due to functional groups, as illustrated in Fig. 9.

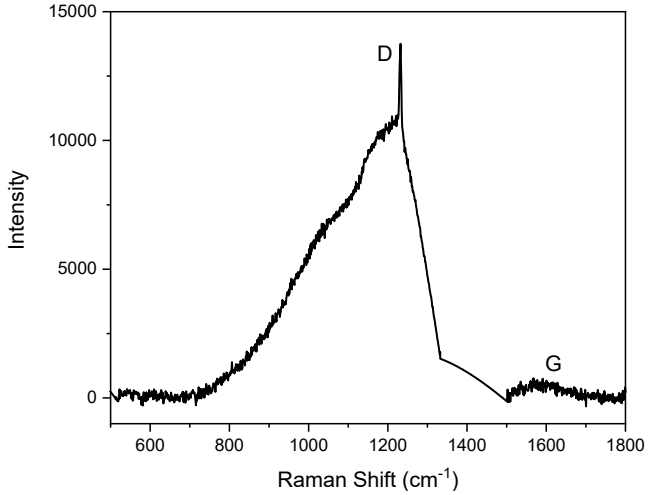

Fig. 7: Raman spectrum of N-CDs 56.

The existence of various functional groups also affected the CDs charge. Zeta potential measurements were employed to assess the CDs charge in a dispersed system[32]. According to the zeta potential characterization (Fig. 8), N-CDs 56 exhibit a positive zeta potential of +105 mV and negative zeta potentials of -29.9 and -92.5 mV, indicating that N-CDs 56 have both positive and negative charges on their surface. However, the positive peak is lower than the negative peak. The higher negative peak is assigned to the prevalence of negative charge functional groups on N-CDs 56 surface, such as alcohol, carboxyl, carbonyl, and imine. On the other hand, the amine functional group contributes to the positive charges observed[33].

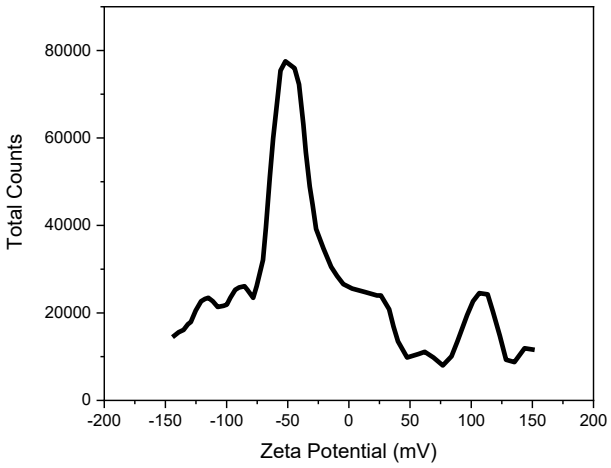

Fig. 8: Zeta potential graph of N-CDs 56

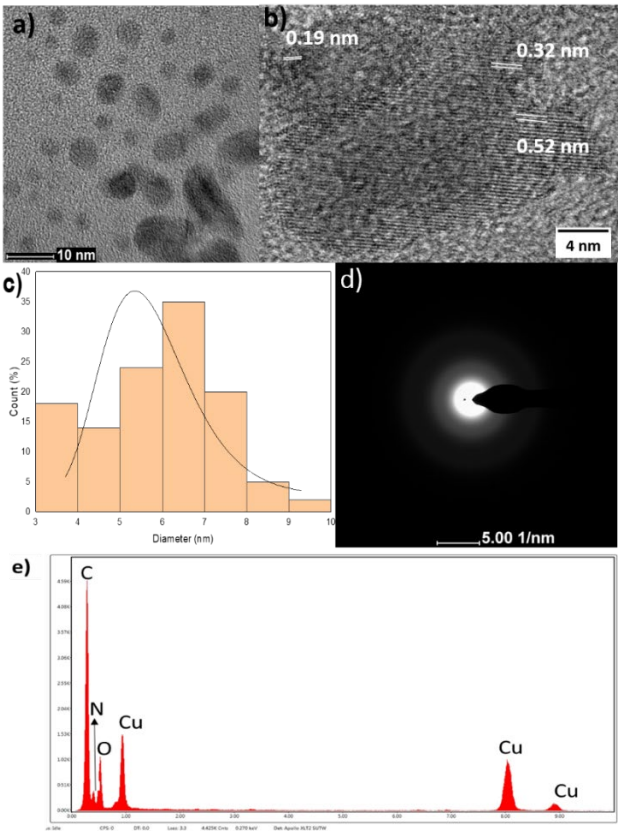

Fig. 9: a) & b) TEM images at various scales, c) graph of size distribution, d) SAED image, and e) EDS of N-CDs 56.

The structure and distribution of particle size from N-CDs 56 were also studied using TEM. In Fig. 9a, the TEM image of N-CDs 56 presented the spherical shape like dots, well distributed and separated from each other without agglomeration formation. Based on Fig. 9b, lattice fringes were observed with d-spacing of 0.52 and 0.32 nm. These d-spacing values are associated with the (002) lattice planes of graphite. An additional d-spacing of 0.19 nm reveals (101) lattice planes belonging to the graphite structure. The graphitic structure is characteristic of CDs structure. This is an agreement with XRD and Raman. The size distribution of N-CDs was calculated using ImageJ and the results are displayed in Fig. 9c. N-CDs have a size ranging from 3.16-9.78 nm with 5.94 nm as the average size. The SAED pattern in Fig. 9d confirmed the amorphous nature of N-CDs. It is consistent with XRD and Raman results, N-CDs have low crystallinity caused by the abundance of functional groups on the CDs surface. From the EDS data in Fig. 9e, N-CDs consist of carbon (55.8%), oxygen (21.7%), and nitrogen (22.5%), indicating the purity of the N-CDs obtained. Based on all the characterizations carried out, it can be concluded that N-CDs have a defective graphite structure due to the presence of functional groups such as O-H, N-H, O-C-O, C=O, and C=N, as shown in Fig. 10. This varied functional group causes N-CDs to form bonds with metal ions, making them potentially applicable as selective and sensitive metal ion sensors[8,13,34].

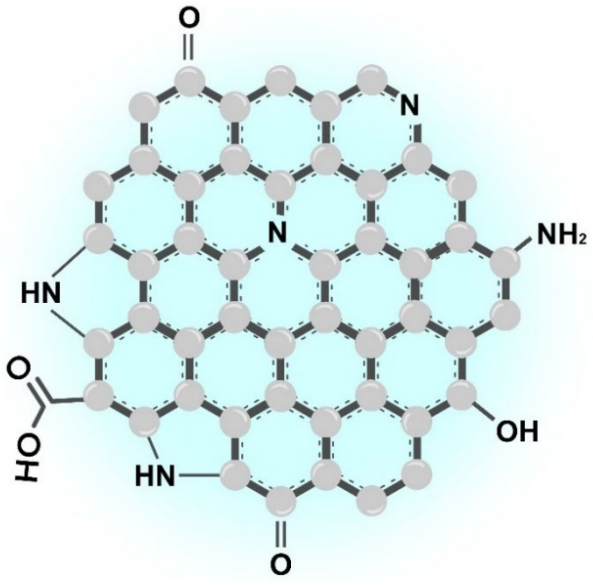

Fig. 10: Illustrated structure of N-CDs 56 (dashed line represents electronic resonances).

3. Conclusion

The synthesis of N-CDs has been successfully achieved using plastic bags as a carbon source and pyrolysis-hydrothermal as the synthesis method. The yield of N-CDs was obtained using variation of H_2O_2 concentration and hydrothermal time ranging from 6.9% to 30.2%. Doping nitrogen with CDs, increasing H_2O_2 concentration to 5 wt%, and extending hydrothermal time to 6 h can increase the fluorescence intensity and quantum yield from 1.2 to 20%. The size of N-CDs ranges from 3.16-9.78 nm and 5.94 nm as the average size. Based on the characterization performed, N-CDs have a graphite structure with defects due to the existence of surface functional groups such as alcohol, carboxyl, carbonyl, amine, and imine. The fluorescence stability test indicated that N-CDs were stable to storage time, the presence of NaCl and PBS. Thus, possible applications for contaminant sensing in wastewater samples and human cells are envisaged.

Acknowledgments

RL acknowledges the PMDSU Scholarships by the Ministry of Education, Culture, Research, and Technology, the Republic of Indonesia. The authors thank Prof. Shin-ichiro Noro and Prof. Yuichi Kamiya for the XRD measurement.

References

1) B. Rusdyanto, F. Imaduddin, and D. Ariawan, “The Tensile Properties of Recycled Polypropylene Filament (rPP) as 3D Printing Material,” Evergreen, 10(1) 489–495 (2023). doi: 10.5109/6782152.
2) H. Koide, T. Seiichi, K. Tamura, W. Jung, H. Nakayama, S. Matsuda, and K. Moroga, “Possibility of Cooperation for a Low Carbon Society: Comparison of the Fukuoka and Busan Metropolitan Cities,” Evergreen, 2(Sep) 21–35 (2010) http://jointfukuoka.seesaa.net/.
3) A. Chamas, H. Moon, J. Zheng, Y. Qiu, T. Tabassum, J.H. Jang, M. Abu-Omar, S.L. Scott, and S. Suh, “Degradation rates of plastics in the environment,” ACS Sustain Chem Eng, 8(9) 3494–3511 (2020). doi:10.1021/acssuschemeng.9b06635.
4) Y. Hu, J. Yang, J. Tian, L. Jia, and J.S. Yu, “Green and size-controllable synthesis of photoluminescent carbon nanoparticles from waste plastic bags,” RSC Adv, 4(88) 47169–47176 (2014). doi:10.1039/c4ra08306g.
5) L. Li, and T. Dong, “Photoluminescence tuning in carbon dots: surface passivation or/and functionalization, heteroatom doping,” J Mater Chem C Mater, 6(30) 7944–7970 (2018). doi:10.1039/c7tc05878k.
6) B.P. de Oliveira, N.U. de C. Bessa, J.F. do Nascimento, C.S. de Paula Cavalcante, R.O. dos S. Fontenelle, and F.O.M. da S. Abreu, “Synthesis of luminescent chitosan-based carbon dots for candida albicans bioimaging,” Int J Biol Macromol, 227 805–814 (2023). doi:10.1016/j.ijbiomac.2022.12.202.
7) N. Tejwan, M. Kundu, N. Ghosh, S. Chatterjee, A. Sharma, T. Abhishek Singh, J. Das, and P.C. Sil, “Synthesis of green carbon dots as bioimaging agent

and drug delivery system for enhanced antioxidant and antibacterial efficacy," Inorg Chem Commun, 139 (2022). doi:10.1016/j.inoche.2022.109317.

8) R. Lestari, T.D. Wahyuningsih, Y. Kamiya, and I. Kartini, "Transforming high-density polyethylene plastic bags into eco-friendly carbon dots for detecting ferric (Fe3+) ions," Diam Relat Mater, 139 110271 (2023). doi:10.1016/j.diamond.2023.110271.
9) S.M.A. Pontes, V.S.F. Rodrigues, S.V. Carneiro, J.J.P. Oliveira, T.A. Moura, A.R. Paschoal, R.A. Antunes, D.R. de Oliveira, J.R. Oliveira, L.M.U.D. Fechine, S.E. Mazzetto, P.B.A. Fechine, and C. da S. Clemente, "One-pot solvothermal synthesis of full-color carbon quantum dots for application in light emitting diodes," Nano-Struct Nano-Objects, 32 100917 (2022). doi:10.1016/j.nanoso.2022.100917.
10) X. Wang, L. Xu, S. Ge, S.Y. Foong, R.K. Liew, W.W. Fong Chong, M. Verma, Mu. Naushad, Y.-K. Park, S.S. Lam, Q. Li, and R. Huang, "Biomass-based carbon quantum dots for polycrystalline silicon solar cells with enhanced photovoltaic performance," Energy, 274 127354 (2023). doi:10.1016/j.energy.2023.127354.
11) R. Lestari, I. Kartini, and T.D. Wahyuningsih, "Effect of Hydrogen Peroxide Concentration to Fluorescence Properties of Carbon Dot from HDPE," Key Eng Mater, 920 106–113 (2022). doi:10.4028/p-x50zy8.
12) M.J. Baari, and R.Y. Pratiwi, "Application of Carbon Dots as Corrosion Inhibitor: A Systematic Literature Review," Indones J Chem, 22(5) 1427-1453 (2022). doi: 10.22146/ijc.72327.
13) Y. Hu, Z. Gao, J. Yang, H. Chen, and L. Han, "Environmentally benign conversion of waste polyethylene terephthalate to fluorescent carbon dots for 'on-off-on' sensing of ferric and pyrophosphate ions," J Colloid Interface Sci, 538 481–488 (2019). doi:10.1016/j.jcis.2018.12.016.
14) A. Kumari, A. Kumar, S.K. Sahu, and S. Kumar, "Synthesis of green fluorescent carbon quantum dots using waste polyolefins residue for Cu2+ ion sensing and live cell imaging," Sens Actuators B Chem, 254 197–205 (2018). doi:10.1016/j.snb.2017.07.075.
15) J. Manioudakis, F. Victoria, C.A. Thompson, L. Brown, M. Movsum, R. Lucifero, and R. Naccache, "Effects of nitrogen-doping on the photophysical properties of carbon dots," J Mater Chem C Mater, 7(4) 853–862 (2019). doi:10.1039/c8tc04821e.
16) K. Chan, and A. Zinchenko, "Aminolysis-assisted hydrothermal conversion of waste pet plastic to n-doped carbon dots with markedly enhanced fluorescence," J Environ Chem Eng, 10(3) (2022). doi:10.1016/j.jece.2022.107749.
17) M. Saikia, T. Das, N. Dihingia, X. Fan, L.F.O. Silva, and B.K. Saikia, "Formation of carbon quantum dots and graphene nanosheets from different abundant carbonaceous materials," Diam Relat Mater, 106 (2020). doi:10.1016/j.diamond.2020.107813.
18) S. Zhu, Y. Song, J. Wang, H. Wan, Y. Zhang, Y. Ning, and B. Yang, "Photoluminescence mechanism in graphene quantum dots: quantum confinement effect and surface/edge state," Nano Today, 13 10–14 (2017). doi:10.1016/j.nantod.2016.12.006.
19) W.J. Fu, Z.X. Peng, Y. Dai, Y.F. Yang, J.Y. Song, W. Sun, B. Ding, H.W. Gu, and X.L. Yin, "Highly fluorescent N doped C-dots as sensor for selective detection of Hg2+ in beverages," Spectrochim Acta A Mol Biomol Spectrosc, 265 (2022). doi:10.1016/j.saa.2021.120392.
20) S.S. Ali, T. Elsamahy, E. Koutra, M. Kornaros, M. El-Sheekh, E.A. Abdelkarim, D. Zhu, and J. Sun, "Degradation of conventional plastic wastes in the environment: a review on current status of knowledge and future perspectives of disposal," Sci Total Environ, 771 (2021). doi:10.1016/j.scitotenv.2020.144719.
21) Z. Tang, W. Chen, J. Hu, S. Li, Y. Chen, H. Yang, and H. Chen, "Co-pyrolysis of microalgae with low-density polyethylene (LDPE) for deoxygenation and denitrification," Bioresour Technol, 311 (2020). doi:10.1016/j.biortech.2020.123502.
22) C. Mickaël, F. Jiahui, R. Mickaël, P. Françoise, and L. Luc, "Influence of carbonization conditions on luminescence and gene delivery properties of nitrogen-doped carbon dots," RSC Adv, 9(6) 3493–3502 (2019). doi:10.1039/c8ra09651a.
23) V. Ramanan, B. Siddaiah, K. Raji, and P. Ramamurthy, "Green synthesis of multifunctionalized, nitrogen-doped, highly fluorescent carbon dots from waste expanded polystyrene and its application in the fluorimetric detection of Au3+ ions in aqueous media," ACS Sustain Chem Eng, 6(2) 1627–1638 (2018). doi:10.1021/acssuschemeng.7b02852.
24) M.I.S. Dela Cruz, N. Thongsai, M.D.G. de Luna, I. In, and P. Paoprasert, "Preparation of highly photoluminescent carbon dots from polyurethane: optimization using response surface methodology and selective detection of silver (I) ion," Colloids Surf A Physicochem Eng Asp, 568 184–194 (2019). doi:10.1016/j.colsurfa.2019.02.022.
25) G. Ma, R. Wang, M. Zhang, Z. Dong, A. Zhang, M. Qu, L. Gao, Y. Wei, and J. Wei, "Solvothermal preparation of nitrogen-doped carbon dots with pet waste as precursor and their application in leads and water detection," Spectrochim Acta A Mol Biomol Spectrosc, 289 (2023). doi:10.1016/j.saa.2022.122178.
26) F. Wu, H. Su, K. Wang, W.K. Wong, and X. Zhu, "Facile synthesis of N-rich carbon quantum dots from porphyrins as efficient probes for bioimaging and biosensing in living cells," Int J Nanomedicine, 12 7375–7391 (2017). doi:10.2147/IJN.S147165.
27) R. Atchudan, T.N.J.I. Edison, S. Perumal, N. Muthuchamy, and Y.R. Lee, "Hydrophilic nitrogen-doped carbon dots from biowaste using dwarf banana

peel for environmental and biological applications," Fuel, 275 (2020). doi:10.1016/j.fuel.2020.117821.
28) J.D. Stachowska, A. Murphy, C. Mellor, D. Fernandes, E.N. Gibbons, M.J. Krysmann, A. Kelarakis, E. Burgaz, J. Moore, and S.G. Yeates, "A rich gallery of carbon dots based photoluminescent suspensions and powders derived by citric acid/urea," Sci Rep, 11(1) (2021). doi:10.1038/s41598-021-89984-w.
29) M. Kaur, N. Mittal, A. Charak, A.P. Toor, and V. Singh, "Rice Husk derived Activated Carbon for the Adsorption of Scarlet RR an Anionic Disperse Dye," Evergreen, 10(1) 438–443 (2023). https://doi.org/10.5109/6782146.
30) M. Todica, T. Stefan, S. Simon, I. Balasz, and L. Daraban, "UV-Vis and XRD investigation of graphite-doped poly(acrylic) acid membranes," Turk J Phys, 38(2) 261–267 (2014). doi:10.3906/fiz-1305-16.
31) I.F. Andhika, T.E. Saraswati, and S. Hastuti, "The structural characteristics of carbon nanoparticles produced by arc discharge in toluene without added catalyst or gases," Evergreen, 7(3) 417–428 (2020). doi:10.5109/4068622.
32) M.R. Zakaria, M.F. Omar, H.M. Akil, and M.M.A.B. Abdullah, "Study of carbon nanotubes stability in different types of solvents for electrospray deposition method," Evergreen, 7(4) 538–543 (2020). doi:10.5109/4150473.
33) A. Saravanan, M. Maruthapandi, P. Das, S. Ganguly, S. Margel, J.H.T. Luong, and A. Gedanken, "Applications of N-doped carbon dots as antimicrobial agents, antibiotic carriers, and selective fluorescent probes for nitro explosives," ACS Appl Bio Mater, 3(11) 8023–8031 (2020). doi:10.1021/acsabm.0c01104.
34) F.D. Sari, Chotimah, Roto, and I. Kartini, "Highly fluorescent nitrogen-doped graphene quantum dots (N-GQDs) synthesized from Pennisetum purpureum for selective and sensitive detection of Fe3+ ions," Mater Res Express, 10(7) 075603 (2023). doi: 10.1088/2053-1591/ace6f6.